Dear Author,

Please, note that changes made to the HTML content will be added to the article before publication, but are not reflected in this PDF.

Note also that this file should not be used for submitting corrections.

MRI molecular imaging using GLUT1 antibody-Fe$_3$O$_4$ nanoparticles in the hemangioma animal model for differentiating infantile hemangioma from vascular malformation

Q1 Chul-Ho Sohn, MD, PhD[a,1], Seung Pyo Park, PhD[b,1], Seung Hong Choi, MD, PhD[b], Sung-Hye Park, MD[c], Sukwha Kim, MD, PhD[d], Lianji Xu, MD, PhD[e], Sang-Hyon Kim, MD[f], Ji An Hur, MD, PhD[g], Jaehoon Choi, MD[h,2], Tae Hyun Choi, MD, PhD[d,*,2]

[a]*Department of Radiology, Seoul National University College of Medicine, Seoul, Republic of Korea*
[b]*Center for Nanoparticle Research, Institute for Basic Science, and School of Chemical and Biological Engineering, Seoul National University, Seoul, Republic of Korea*
[c]*Department of Pathology, Seoul National University College of Medicine, Seoul, Republic of Korea*
[d]*Department of Plastic and Reconstructive Surgery, Institute of Human-Environment Interface Biology, Seoul National University College of Medicine, Seoul, Republic of Korea*
[e]*Department of Plastic and Reconstructive Surgery, Beijing Tongren Hospital, Capital Medical University, People's Republic of China*
[f]*Department of Internal Medicine, Keimyung University Dongsan Medical Center, Daegu, Republic of Korea*
[g]*Department of Internal Medicine, School of Medicine, Yeungnam University, Daegu, Republic of Korea*
[h]*Department of Plastic and Reconstructive Surgery, Keimyung University School of Medicine, Daegu, Republic of Korea*

Q2 ## Abstract

The purpose of this study is to evaluate the efficacy of glucose transporter protein 1 (GLUT1) antibody-conjugated iron oxide nanoparticles (Fe$_3$O$_4$ NPs) as magnetic resonance imaging (MRI) molecular imaging agents for differentiating infantile hemangioma from vascular malformation in the hemangioma animal model. The conjugation of Fe$_3$O$_4$ NPs with anti-GLUT1 antibodies leads to a significantly increased uptake of NPs by human umbilical vein endothelial cells. MRI imaging following the intravenous injection of GLUT1 antibody-Fe$_3$O$_4$ NPs yielded a significantly lower signal intensity than did unconjugated Fe$_3$O$_4$ NPs. Upon histological examination of the GLUT1 antibody-Fe$_3$O$_4$ NPs, Prussian blue-stained NPs were identified in CD31-positive endothelial cells of hemangioma. In contrast, when treated with unconjugated Fe$_3$O$_4$ NPs, Prussian blue-stained NPs were found in macrophages rather than in endothelial cells. No organ damage or structural malformations were found. GLUT1 antibody conjugation can effectively target the injected Fe$_3$O$_4$ NPs to GLUT1-positive tumor cells in infantile hemangioma.
© 2014 Published by Elsevier Inc.

Key words: Iron oxide nanoparticle; GLUT1; Infantile hemangioma; MRI

Background

Vascular anomalies comprise vascular tumors and vascular malformations. A vascular tumor is represented by infantile hemangioma, which is the most common tumor of infancy, and proliferative lesions characterized by increased endothelial cell turnover. These tumors usually appear after birth, grow rapidly, and involute over the years. Therefore, surgery or treatment is not normally required except for in complications such as ulceration, bleeding, and functional impairments such as obstruction of the visual axis or airway.

Vascular malformations are errors in morphogenesis populated by a stable, mature vascular endothelium. Although not always obvious, these are present at birth, grow commensurately with the child, and do not involute. Therefore, they usually require surgery or embolization.[1]

The differential diagnosis of two diseases is mainly dependent on careful history taking, physical examination, and radiologic images such as ultrasound, computed tomogram (CT), and magnetic resonance imaging (MRI). However, in a number of cases, the differential diagnosis is difficult because the radiologic images do not help differentiate infantile hemangioma from vascular malformation.[2]

Based on recent, rapid developments in nanotechnology, nanoparticles have yielded a new collection of contrast agents for the field of in vivo molecular imaging. Among these, iron oxide nanoparticles (Fe_3O_4NPs) are representative MRI imaging nanoparticles. Fe_3O_4 NPs exhibit better biocompatibility than commonly-used gadolinium-based agents. Fe_3O_4 NPs are known to be biologically well tolerated, and their toxicity, metabolism, and pharmacokinetics are well studied.[3] Moreover, gadolinium-based agents have dangerous side effects, such as nephrogenic systemic fibrosis.[4] Because of their magnetic properties, Fe_3O_4 NPs exhibit higher sensitivity than gadolinium-based agents; therefore, Fe_3O_4NPs can be utilized as T2 MRI contrast agents.[5] By utilizing the large surface-area-to-volume ratio of these NPs, antibody-conjugated Fe_3O_4 NPs can act as an effective probe for specific diseases.[6] Additionally, recent advances in synthetic methods of magnetic NPs make it possible to yield ultrasensitive MRI contrast agents having high relaxivity, which can provide an accurate diagnosis based on detailed anatomic information.[7]

Glucose transporter protein 1 (GLUT1) is only expressed in endothelial cells of infantile hemangioma, not vascular malformation. Therefore, GLUT1 is widely used as a differential diagnosis marker in pathology departments.[8] Based on this, we conjugated a GLUT1 antibody as a targeting moiety to Fe_3O_4 NPs as an MRI imaging group for differentiating infantile hemangioma from vascular malformation. The purpose of this study is to evaluate the efficacy of GLUT1 antibody-Fe_3O_4 NPs as MRI molecular imaging agents in the hemangioma animal model.

Methods

Animals

BAlb/c nude mice were purchased from SAMTACO (Osan, Korea). All the animals were kept in separate cages under controlled temperature (24-26 °C), humidity, and photoperiod conditions. All the experiments in this study were performed in accordance with the guidelines for animal research from the National Institutes of Health and were approved by the Institutional Animal Care and Use Committee and the institute of review board at Seoul National University Hospital in Seoul, Korea (10–0040, H-1003-002-310).

Preparation of amine-functionalized Fe_3O_4 NPs encapsulated by PEG-phospholipids

Iron chloride (FeCl$_3$ · 6H$_2$O, 98%), oleic acid (technical grade, 90%), and 1-octadecene (technical grade, 90%) were purchased from Aldrich. Sodium oleate (95%) was purchased from TCI. 1,2-Distearoyl-*sn*-glycero-3-phosphoethanolamine-*N*-[methoxy(polyethylene glycol)-2000] (mPEG-2000PE) and 1,2-distearoyl-*sn*-glycero-3-phosphoethanolamine-*N*-[amino(polyethylene glycol)-2000] [DSPE-PEG(2000)Amine] were purchased from Avanti Polar Lipids, Inc. All the reagents were used as received.

Fe_3O_4 NPs (10 nm in size) were synthesized by using a previously reported method.[9] An iron-oleate precursor was prepared from the reaction of iron chloride (FeCl$_3$ · 6H$_2$O, 98%; Aldrich) and sodium oleate (technical grade, 90%; Aldrich). The thermal decomposition of the iron-oleate precursors in a high-boiling solvent produced Fe_3O_4 NPs. In a typical reaction, 40 mmol of iron-oleate precursor and 20 mmol of oleic acid were dissolved in 200 g of 1-octadecene. The reaction mixture is heated to 320 °C at a constant heating rate of 3.3 °C/min and subsequently maintained at that temperature for 30 min. The resulting solution was then cooled to room temperature. Fe_3O_4 NPs were precipitated by adding ethanol and retrieved by centrifugation. The synthesized NPs were characterized by transmission electron microscopy (TEM). The TEM images were obtained on a Jeol EM-2010 microscope.

Amine-functionalized Fe_3O_4 NPs encapsulated by PEG-phospholipids were prepared by the method described previously with a number of modifications.[10] Fe_3O_4 NPs (10 mg) in chloroform were mixed with a mixture of 16 mg 1,2-distearoyl-*sn*-glycero-3-phosphoethanolamine-*N*-[methoxy(polyethylene glycol)-2000] (mPEG-2000PE; Avanti Polar Lipids, Inc) and 4 mg 1,2-distearoyl-*sn*-glycero-3-phosphoethanolamine-*N*-[amino(polyethylene glycol)-2000] [DSPE-PEG(2000)Amine; Avanti Polar Lipids, Inc] in chloroform. After evaporating the solvent, the mixture was incubated at 60 °C in vacuum for 30 min. The addition of water (10 ml) resulted in a black, transparent suspension. After filtration using a 0.2 μm cellulose acetate syringe filter, excess PEG-phospholipids were removed by ultracentrifugation. The concentrations of the Fe_3O_4 NPs were measured and calculated using inductively-coupled plasma atomic emission spectroscopy (ICP-AES) using an ICPS-7500 spectrometer (Shimadzu). The hydrodynamic diameter of the nanoparticles dispersed in water was measured with a particle size analyzer (ELS-Z2, Otsuka).

Conjugation of GLUT1 antibodies to Fe_3O_4 NPs

Nine hundred micrograms of GLUT1 Ab (Pierce, #MA1-37783) was dissolved in 500 μl of phosphate-buffered saline (PBS, pH 7.2) and mixed with 60 μl of *N*-succinimidyl *S*-acetylthioacetate (SATA) in dimethyl sulfoxide (1.5 mg/ml).

After mixing and incubation at room temperature (RT) for 30 min, 120 μl of 0.5 M hydroxylamine in PBS was added, and the solution was incubated for 2 hours at RT. Thiolated GLUT1 Ab was purified using PD-10 desalting columns (GE), and 1.0 ml of the flow-through was collected. Amine-functionalized Fe_3O_4 NPs (5 mg) were mixed with 25 μl of succinimidyl 4-[N-maleimido-methyl] cyclohexane-1-carboxylate (Pierce, #22360) (SMCC) in dimethyl sulfoxide (134 ug/ml). The reaction mixture was incubated for 30 min at RT. Maleimido-Fe_3O_4 NPs were purified with a PD-10 desalting column (GE, #17-0851-01). Thiolated GLUT1 Ab (1 ml) and 0.6 ml of maleimido-Fe_3O_4 NPs (5 mg/ml) were mixed and incubated for 2.5 hours at 4 °C, and the GLUT1-conjugated Fe_3O_4 NPs were isolated by gel filtration with a Sephacryl S-200 (GE, #17-0584-01).

In vitro assay using HUVECs

Prior to the in vivo imaging study, to test the in vitro toxicity, we used human umbilical vein endothelial cells (HUVECs, Lonza Biologics Inc., Portsmouth, NH, USA) to mimic endothelial cells of human infantile hemangioma. HUVECs also express GLUT1 antigens in the same manner as the endothelial cells of infantile hemangioma.[11]

HUVECs were seeded at 30,000 cells/well in 48-well plates. To examine the viability of HUVECs in response to Fe_3O_4 NPs and GLUT1 antibody-Fe_3O_4 NPs, the cells were treated in the absence of Fe_3O_4 NPs or with various concentrations of Fe_3O_4 NPs and GLUT1 antibody-Fe_3O_4 NPs for 24 hours. Cell viability was subsequently determined by the CCK assay (Cell Proliferation Assay Kit; Dojindo, Japan). In addition, the labeling efficiency of the Fe_3O_4 NPs and the GLUT1 antibody-Fe_3O_4 NPs was confirmed by Prussian blue stain assay following incubation with the Fe_3O_4 NPs and the GLUT1 antibody-Fe_3O_4 NPs for 9 hours. Prussian blue stain images were captured using a Leica inverted microscope (Leica Microsystems GmbH, Wetzlar, Germany) and the Leica Application Suite software. The staining parameters were evaluated at 200× magnification, and four areas of high-density staining were selected for the quantitative analysis. The images were quantitatively analyzed using the Leica Application Suite Image program.

$$Optical\ density\ mean(\%)$$
$$= Positive\ stained\ area(\mu m^2)/Total\ area(\mu m^2) \times 100$$

Optical density means are expressed as the mean ± SD. Student's t test was used to compare data from two groups (positive control group and experimental group). The level of significance was set at $P < 0.05$.

Infantile hemangioma animal model

The infantile hemangioma animal model was utilized as in previous reports by Tang et al. In summary, the infantile hemangioma tissue was obtained surgically from three children who were referred to our department for a rapidly growing mass. Informed consent was obtained from the parents for experimental investigations under the approval by the Institutional Review Board of Seoul National University Hospital in Seoul, Korea.

The cutaneous portions were removed from the hemangioma tissue, and the remainder was cut into small pieces of approximately $5 \times 4 \times 3$ mm. Under anesthesia, eight nude mice were implanted with the tumor pieces subcutaneously.[12]

Histologic examination of tissue sections

Formalin-fixed, paraffin-embedded tissues were sectioned to a thickness of 4 μm and stained with hematoxylin and eosin.

Immunohistochemistry

Deparaffinized sections were pre-incubated with 10% horse serum. The sections were then incubated with the polyclonal antibody against human CD31 (abcam, Cambridge, USA) or GLUT-1 (abcam, Cambridge, UK) at 37 °C for 1 hour, followed by incubation with a secondary antibody (DAKO) for 1 hour. Antibody binding was detected using 3,3′-diaminobenzidine (DAB; DAKO). Following the immunohistochemistry, a number of sections were also stained with Prussian blue to investigate the colocalization of CD31 and iron deposition.

MRI in the hemangioma animal model

Four weeks after the hemangioma tissue implantation, the nude mice were subjected to the MRI. An in vivo MRI was performed using a clinical 3 T MR scanner (MAGNETOM Tim Trio; Siemens Medical Solutions, Erlangen, Germany) with a 4-channel wrist coil. The imaging protocol consisted of a sagittal 3D T2*-weighted gradient-recalled-echo (GRE) sequence with the following imaging parameters: TR/TE = 40/22 milliseconds, flip angle = 12°, FOV = 49×70 mm, matrix = 256×180, slice thickness = 1 mm, and the number of excitations = 3. Before the injection of the molecular imaging agents, the control group and the experimental group were scanned by MRI. Next, the control group was injected intravenously with Fe_3O_4 NPs (10 μg/g), and the experimental group with GLUT1 antibody-Fe_3O_4 NPs (10 μg/g). Twenty-four hours following the injection, both groups were also scanned using an MRI machine. The MRI data were digitally transferred from a PACS workstation to a personal computer and processed with ImageJ (available at http://rsb.info.nih.gov/ij/).

ROIs that contained the entire hemangioma were drawn in each section of the T2*-weighted GRE images. Using software developed in-house, the data acquired from each slice were summated to derive the pixel-by-pixel SI (signal intensity) values for the entire hemangioma. Previous studies have shown that adipose cells mainly express GLUT-4, not GLUT-1[13,14]; therefore, the pixel-by-pixel SI values were then normalized to the fatty area of the posterior neck to cancel the SI fluctuations related to variations in the technical parameters between the MRI sequences obtained both pre- and post-injection of the Fe_3O_4 NPs or GLUT1 antibody-Fe_3O_4 NPs. The SI of the fatty area was measured within a single ROI, measuring 3-5 mm^2, placed in the posterior neck. Finally, SI histograms for the hemangiomas were plotted using a bin size of 1% with the normalized SI (nSI) value (i.e., normalized SI value (%) = [SI of hemangiomas]/[SI of fatty areas] × 100) on the x-axis, and the percentage of the total lesion volume was expressed on the y-axis by dividing the frequency of each bin by the total percentages of pixels analyzed.
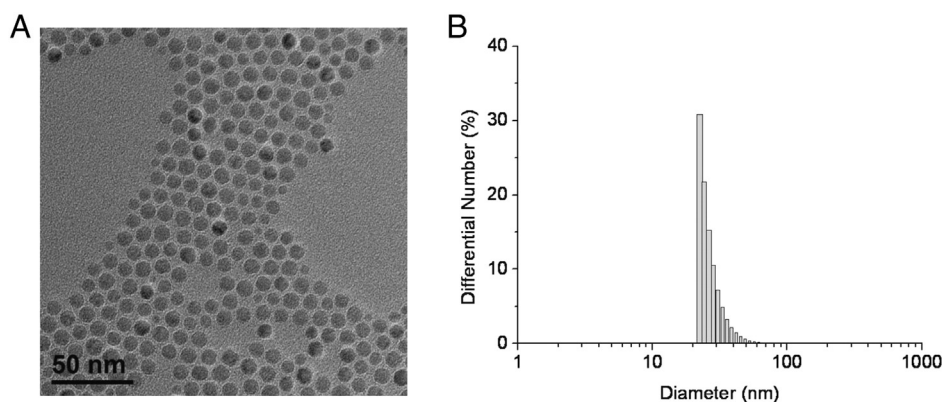
Figure 1. (**A**) Transmission electron microscopy (TEM) image of Fe$_3$O$_4$ NPs dispersed in hexane. The average particle size is 10 nm. (**B**) Dynamic light scattering (DLS) histogram for water-dispersible iron oxide nanoparticles coated with PEG-phospholipids. The hydrodynamic diameter is 27.0 ± 6.4 nm.

245   A baseline pixel histogram using the nSI of a hemangioma was
246 created from the MR images obtained before the injection of the
247 Fe$_3$O$_4$ NPs or the GLUT1 antibody-Fe$_3$O$_4$ NPs to establish the
248 minimum nSI in the absence of any Fe. On the MR images
249 obtained 24 hours after the injection of the Fe$_3$O$_4$ NPs or GLUT1
250 antibody-Fe$_3$O$_4$ NPs, the percentages of pixels in the hemangi-
251 omas below the minimum nSI threshold were summated and
252 reported as the black pixel count (%) for the Fe$_3$O$_4$ NPs or GLUT1
253 antibody-Fe$_3$O$_4$ NPs hypo-intensity.
254   We compared the mean normalized SIs of the pre-injection of
255 both groups (control and experimental groups) to demonstrate the
256 non-difference (similarity) of the hypo-intensity of the hemangi-
257 oma. We also compared the mean normalized SIs of the pre-
258 injection with the post-injection to evaluate the effect in both
259 groups. Finally, we compared the mean percentages of the pixels
260 below the minimum nSI threshold after the injection in both groups
261 to evaluate the effect of the GLUT1 antigen-antibody reaction.
262   Furthermore, signal to-noise ratio (SNR) and contrast-to-noise
263 ratio (CNR) were calculated using the following equations[15-18]:

$$SNR = SI_{hemangiomas}/noise_{(air)}$$
$$CNR = |SI_{hemangiomas} - SI_{fatty\ areas}|/\sigma_{noise(air)}$$

265 where SI$_{hemangiomas}$ is the average signal intensity of the
266 hemangiomas, $\sigma_{noise(air)}$ is the standard deviation of the background
267 noise measured at the air with a ROI of 3-5 mm^2, and SI$_{fatty\ areas}$ is
268 the average signal intensity of the fatty area of the posterior neck.

269 **Results**

270 *Preparation of amine-functionalized Fe$_3$O$_4$ NPs*

271   Figure 1, *A* shows the TEM image of the as-synthesized iron
272 oxide nanoparticles (Fe$_3$O$_4$ NPs). The 10 nm-sized Fe$_3$O$_4$ NPs
273 were synthesized through thermal decomposition of iron oleates by
274 the "heat-up process", which is very reproducible, environmentally
275 friendly, and can be readily adapted for large scale production. To
276 render hydrophobic Fe$_3$O$_4$ NPs water-dispersible, the NPs were
277 encapsulated by amphiphilic PEG-phospholipids. After encapsu-
278 lation with PEG-phospholipids, the dynamic light scattering (DLS)
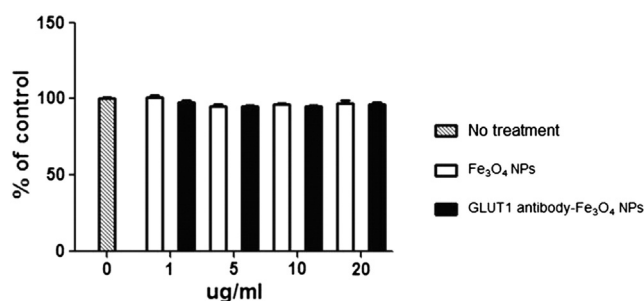279 data showed that the Fe$_3$O$_4$ NPs were dispersed in water without

Figure 2. Viability of human umbilical vein endothelial cells (HUVECs) in response to Fe$_3$O$_4$ NPs and GLUT1 antibody-Fe$_3$O$_4$ NPs. There was no significant difference in the viabilities of HUVECs between the negative control groups (no treatment), Fe$_3$O$_4$ NPs, and the GLUT1 antibody-Fe$_3$O$_4$ NP-treated groups ($P < 0.05$, Kruskal–Wallis test).

any detectable aggregation (Figure 1, *B*). The DLS data also 280
revealed that the overall diameter of the Fe$_3$O$_4$ NPs increased by 281
approximately 17 nm, demonstrating the monolayer-thick encap- 282
sulation of the PEG-phospholipid. 283

Enhanced Uptake of Fe$_3$O$_4$ NPs in Endothelial Cells by GLUT1 284
Antibody Conjugation 285

     When a cholecyctokinin (CCK) assay was performed 286
24 hours later to compare the viability of the HUVECs, there 287
was no significant difference between the untreated and Fe$_3$O$_4$ 288
NPs or GLUT1 antibody-Fe$_3$O$_4$ NP-treated groups (Figure 2), 289
even at a concentration of 20 µg/ml. 290
     As the negative control, HUVECs that were cultured in the 291
absence of NPs had no positive staining in Prussian blue stain 292
(Figure 3, *A*). In the cytoplasm of the Fe$_3$O$_4$ NP-treated cells, 293
tiny blue dots were easily identifiable (Figure 3, *B*). Moreover, 294
the staining intensity was obviously enhanced in GLUT1 295
antibody-Fe$_3$O$_4$ NP-treated cells (Figure 3, *C*). To compare 296
these differences more quantitatively, the optical density was 297
measured. In GLUT1 antibody-Fe$_3$O$_4$ NP-treated cells, it was 298
two-fold higher than that of the Fe$_3$O$_4$ NP-treated cells (Figure 3, 299
D). This result indicates that the GLUT1 conjugation into Fe$_3$O$_4$ 300
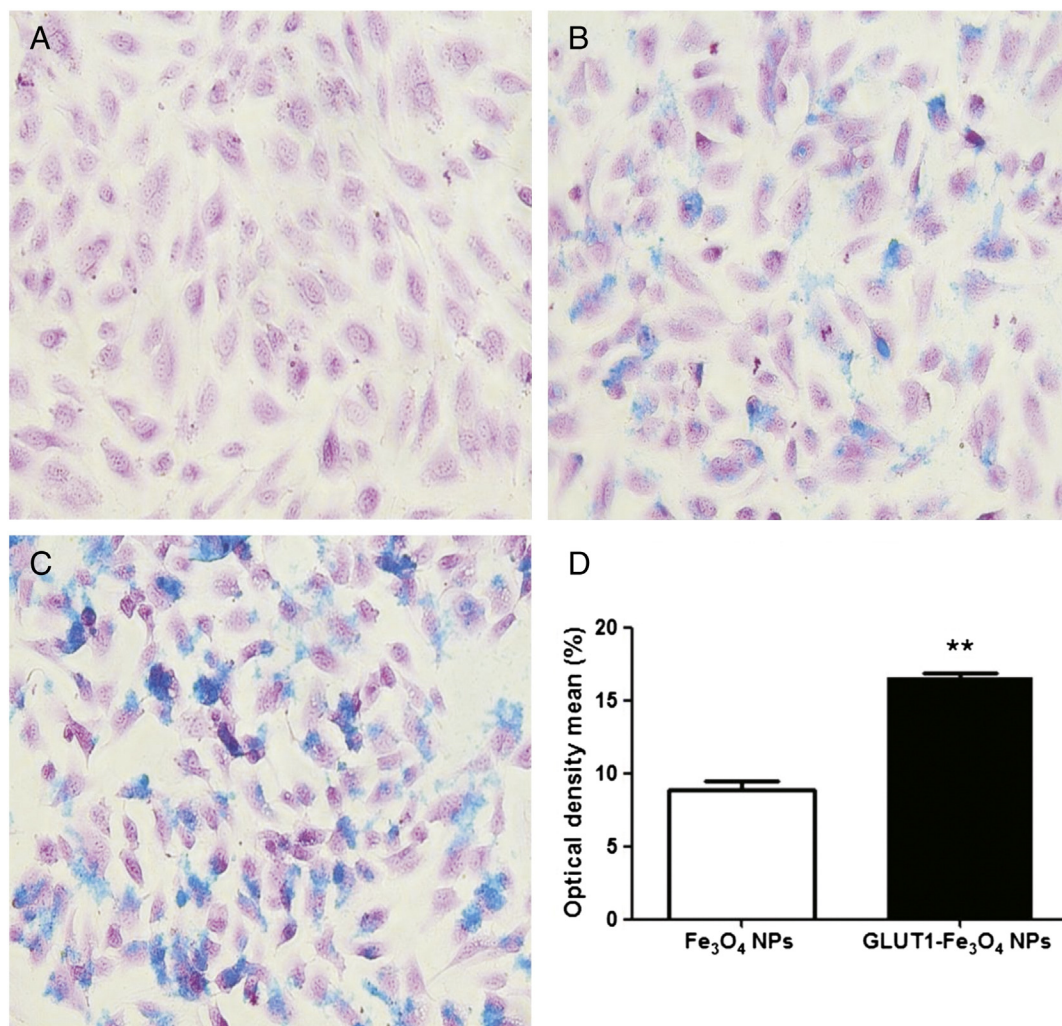NPs significantly enhanced the uptake of NPs by the HUVECs. 301

Figure 3. In vitro Prussian blue staining for the negative control group (no Fe$_3$O$_4$ NPs) (**A**) the positive control group (Fe$_3$O$_4$ NPs) (**B**) and the experimental group (GLUT1 antibody-Fe$_3$O$_4$ NPs) (**C**). In the experimental group, substantially higher number of positive stains was observed. (**D**) Optical density means of Prussian blue staining for quantitative analyses. The bar graph shows the average percentage of positive stained area. **, $P < 0.001$; magnification, ×200.

Development of animal model of infantile hemangioma

The grafts survived in all of the mice. The graft size did not change during the first 2 weeks, and they subsequently shrank by a small amount over the following 2 weeks. In addition, the grafts slowly involuted. Therefore, we used the mice at 4 weeks post-transplantation for further study.

At the histologic examination of the hemangioma tissue 4 weeks following grafting, the tumor consisted of immature capillaries with tiny lumens lined by plump endothelial cells with an outer concentric pericyte layer. Plump, rapidly-dividing endothelial cells formed tightly packed sinusoidal channels. The parenchymal cells assembled in nests or lobules, and there were multiple irregular capillaries within the nests or lobules (Figure 4, *A* and *B*). Immunohistochemical staining demonstrated that the plump endothelial cells expressed both GLUT1 and CD31 in high intensity (Figure 4, *C* and *D*). All these histological features are identical to typical infantile hemangioma in the proliferative phase, indicating that our hemangioma model was identical to infantile hemangioma.

In vivo imaging of infantile hemangioma in animal model

In T2*-weighted GRE MR images of the mice with hemangiomas, the mean normalized SIs of pre-injection of both groups were not significantly different ($P = 0.5626$, Mann–Whitney Test), which meant that both groups had similar hypo-intensity in an MRI (Table 1).

The mean normalized SIs of the pre- and post-Fe$_3$O$_4$ NPs injection in the control group ($n = 4$) were 202 ± 19 and 183 ± 7, respectively. The mean normalized SIs of the pre- and post-GLUT1 antibody-Fe$_3$O$_4$ NP injection in the experimental group ($n = 4$) were 209 ± 10 and 111 ± 11, respectively. The mean normalized SIs for the post-injection were significantly smaller than that for the pre-injection in the experimental group ($P = 0.0286$, Mann–Whitney test), which meant that the GLUT1 antibody-Fe$_3$O$_4$ NPs were effective in lowering the signal density of the hemangioma in the MRI. However, the mean normalized SIs of the post-injection were not significantly smaller than that of the pre-injection in the control group (Table 1).

The mean percentages of pixels below the minimum nSI threshold following the injection in the experimental groups
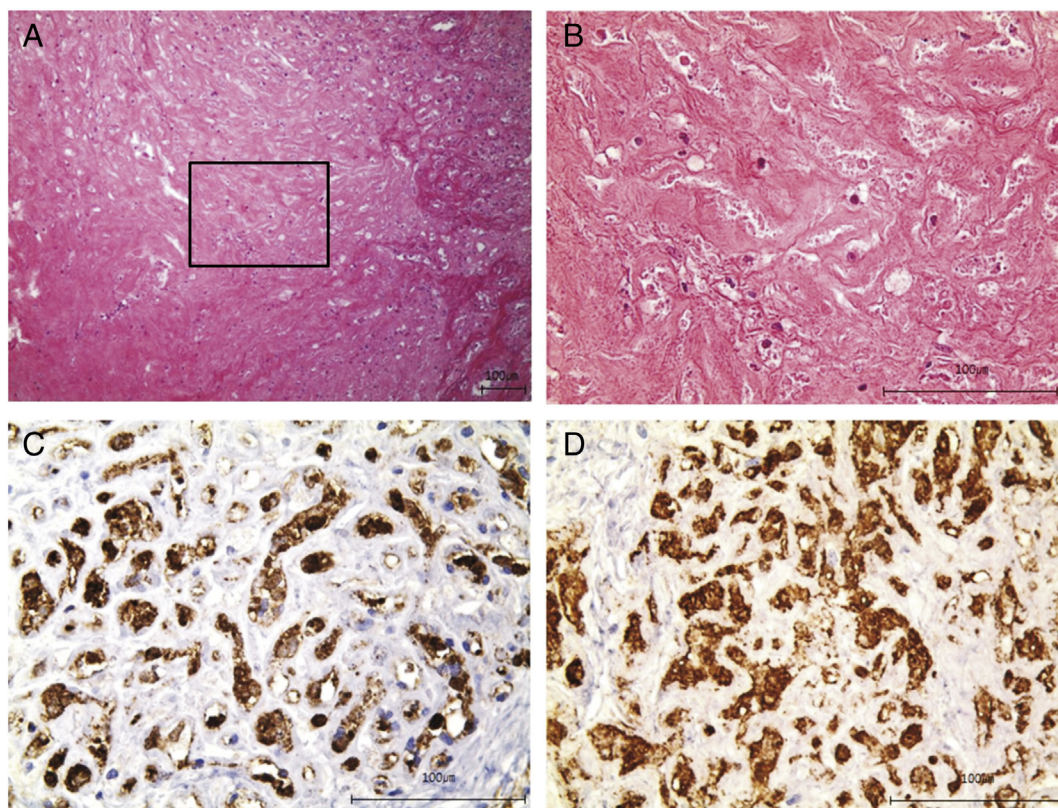
Figure 4. H&E staining and immunohistochemistry of the hemangioma in the animal model. (**A and B**) There were several immature capillaries with tiny lumens lined by plump endothelial cells with an outer concentric pericyte layer. Plump, rapidly-dividing endothelial cells formed tightly packed sinusoidal channels. The parenchymal cells assembled in nests or lobules, and there were multiple irregular capillaries within the nests or lobules. Plump endothelial cells were also strongly stained with GLUT1 (**C**) and CD31 (**D**) immunohistochemistry. Magnification: A ×100, others ×400.

Table 1
Values in T2*-weighted gradient-recalled-echo magnetic resonance images of the mice with hemangiomas.

Groups	Mean normalized SI			Pixels below the minimum nSI threshold after injection (%)
	Pre-injection	Post-injection	P value	
Control group	202 ± 19	183 ± 7	0.1143	12.2 ± 4.2
Experimental group	209 ± 10	111 ± 11	0.0286*	50.8 ± 13.6
P value	0.5626	0.0286*		0.0286*

Note. Data are means ± standard deviations.
* Indicates a statistically significant difference.

(50.8 ± 13.6%) were significantly higher than that in the control group (12.4 ± 4.2%) ($P = 0.0286$, Mann–Whitney test), which meant that the hypo-intensities in the experimental group were significantly higher than in the control group (the GLUT1 antibody-Fe_3O_4 NPs were effective in MRI) (Table 1, Figure 5, *A* and *B*).

In terms of both SNR and CNR, the only experimental group showed statistically significant decreases in mean values after the injection of the GLUT1 antibody-Fe_3O_4 NPs ($P = 0.0286$, Mann–Whitney test) (Table 2).

To investigate the types of cells that take up the intravenously-injected Fe_3O_4 NPs, endothelial cells of the hemangioma were immunohistochemically stained with an anti-CD31 antibody (Figure 6, *A* and *B*, brown color). In the mice that received unconjugated Fe_3O_4 NPs, Prussian blue-stained iron particles were found in the macrophages rather than in the endothelial cells (Figure 6, *A*).This was in sharp contrast to the mice that received GLUT1 antibody-Fe_3O_4 NPs. In these mice, Prussian blue-stained iron particles were easily identifiable in CD31-positive endothelial cells (Figure 6, *B*). Taken together with the in vitro HUVEC study, these results showed that GLUT1 antibody conjugation is able to effectively target the injected Fe_3O_4 NPs to GLUT1-positive tumor cells in infantile hemangioma.

In vivo toxicity test of GLUT1 antibody-Fe_3O_4 NPs to the mice organs

To determine the organ toxicity of GLUT1 antibody-Fe_3O_4 NPs, the mice (ICR, Orientbio, seongnam, Korea) were serially sacrificed for 6 weeks following the NP injections (10 mg/kg), and the histological changes were observed under a light microscope following hematoxylin and eosin staining. As in the control group, the mice received only PBS. No organ damages or structural malformations were found during the short (1 day after the injection) to long term (6 weeks after the injection) follow-up in the experimental groups, compared to the control group, which proved that there was no organ toxicity.
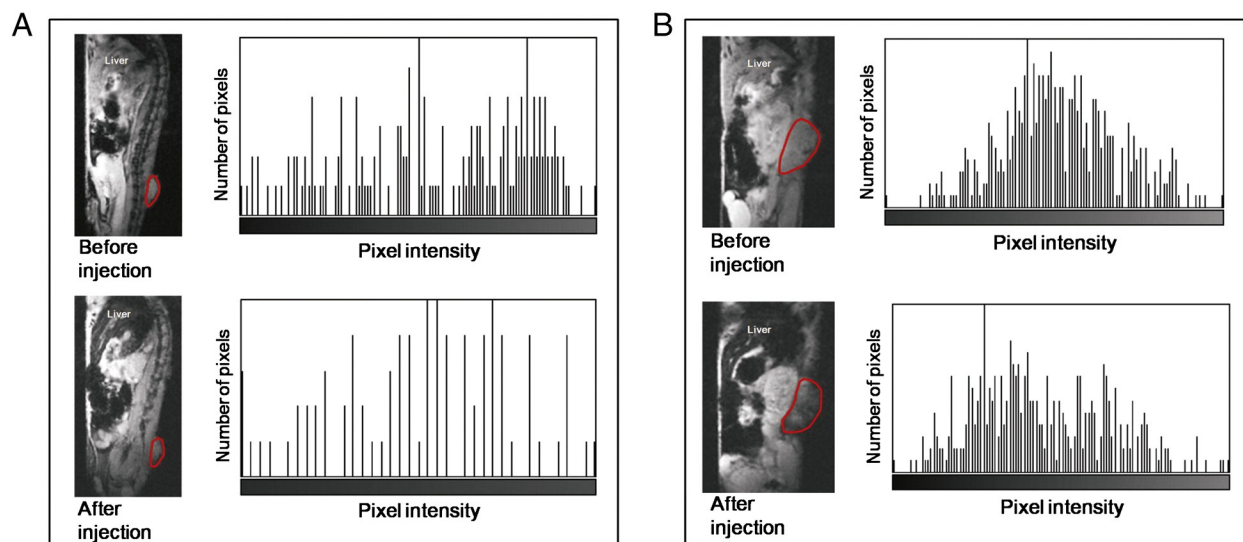
Figure 5. Sagittal T2*-weighted, gradient-recalled-echo (GRE) magnetic resonance (MR) images were taken before and 24 hours after the intravenous administration of Fe_3O_4 NPs (**A**) and GLUT1 antibody-Fe_3O_4 NPs (**B**). The hypointensities from both were detected within the hemangiomas 24 hours after injection. The hypo-intensity means Fe_3O_4 NPs with or without GLUT1 antibodies had been taken up within the hemangiomas. The histograms show very few pixels in the hemangioma after the injection of Fe_3O_4 NPs fell below the threshold (**A**). Notably, substantially more pixels fell below the threshold value after the injection of GLUT1 antibody-Fe_3O_4 NPs (**B**). The percentages of hypointense pixels within the hemangioma of the mice treated with Fe_3O_4 NPs and the GLUT1 antibody-Fe_3O_4 NPs were 8.3 and 56.6%, respectively.

Table 2
Signal-to-noise ratio and contrast-to-noise ratio of the hemangiomas.

Groups	Signal-to-noise ratio			Contrast-to-noise ratio		
	Pre-injection	Post-injection	P value	Pre-injection	Post-injection	P value
Control group	39.3 ± 1.9	35.7 ± 2.2	0.0571	19.8 ± 1.7	16.2 ± 1.5	0.0571
Experimental group	38.1 ± 2.2	18.1 ± 1.3	0.0286*	18.3 ± 1.9	1.8 ± 1.1	0.0286*
P value	0.4679	0.0286*		0.2649	0.0286*	

Note. Data are means ± standard deviations.
* Indicates a statistically significant difference.

Discussion

Infantile hemangioma usually does not require surgery or treatments, except for in the case of complications such as ulceration, bleeding, and functional impairments because it will involute over the years. In contrast, vascular malformation usually requires treatment or surgery because of its commensurate growth with the child. Therefore, the differential diagnosis is very important. In a number of cases, however, the differential diagnosis is very difficult, even though an MRI is performed. These limitations motivate us to develop a molecular imaging technique to differentiate infantile hemangioma from vascular malformations.

In the present study, to overcome this type of limitation of conventional MRI, we used anti-GLUT1 antibodies as targeting tools for infantile hemangioma, and conjugation of this antibody to Fe_3O_4 NPs allowed for a more accurate differential diagnosis of infantile hemangioma from vascular malformation by MRI.

Glucose transporters are a large group of membrane proteins that facilitate the transport of glucose over a plasma membrane. GLUT1 was the first glucose transporter to be characterized.

Under a pathologic condition, GLUT1 expression in the endothelial cells is crucial for the differential diagnosis of infantile hemangioma from vascular malformation because GLUT1 is positive in 100% of infantile hemangioma endothelial cells and negative in vascular malformations including venous, lymphatic, capillary, and arteriovenous malformations. Therefore, the immunohistochemistry of GLUT1 is widely used for differential diagnosis between infantile hemangioma and vascular malformation in the pathology.[8] Based on this, we conjugated GLUT1 antibodies to Fe_3O_4 NPs as MRI molecular imaging agents to differentiate infantile hemangioma from vascular malformation in such cases.

As previously described, the benefit of using Fe_3O_4 NPs is well studied, and it allows for a proper biosafety comparison with other imaging probes (less toxic, FDA approval). Therefore, this material is applicable to clinical demonstrations.

In general, Fe_3O_4 NPs are spontaneously taken up by mammalian cells. This was also the case in HUVECs. When HUVECs were cultured in the presence of Fe_3O_4 NPs in culture media, Fe_3O_4 NPs were observed in the cytoplasm of HUVECs.
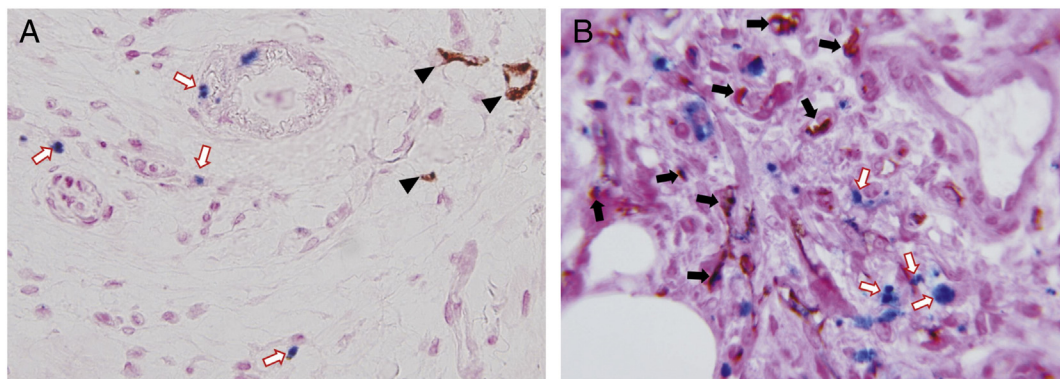
Figure 6. Histologic examinations of hemangiomas 24 hours after the injection of nanoparticles (NPs). (**A**) Control group. Black arrow heads indicate the positive staining of endothelial cells as brown in the CD31 immunohistochemistry, and blank arrows with red outlines indicate phagocytosis of Fe_3O_4 NPs by macrophages (blue in Prussian blue stain). (**B**) Experimental group. The number of positive cells in Prussian blue stain is greater than for the control group. Black arrows indicate the double staining of endothelial cells as brown in the CD31 immunohistochemistry and blue in the Prussian blue stain. This means that endothelial cells in the experimental group take up more Fe_3O_4 NPs through the GLUT1 antigen-antibody reaction. Blank arrows with red outlines indicate phagocytosis of GLUT1 antibody-Fe_3O_4 NPs by macrophages. Magnification: A ×400, B ×1000.

Under this culture condition, the conjugation of Fe_3O_4 NPs with anti-GLUT1 antibodies led to a significantly increased uptake of NPs in HUVECs. Moreover, this targeting effect of anti-GLUT1 antibodies was also demonstrated for an in vivo mouse model of human infantile hemangioma. In hemangioma tissue excised 24 hours following the intravenous injection of anti-GLUT1 antibody-Fe_3O_4 NPs, Prussian blue-stained NPs were identified in CD31-positive endothelial cells of hemangioma. In contrast, when treated with unconjugated Fe_3O_4 NPs, Prussian blue-stained NPs were found in macrophages rather than endothelial cells. MRI imaging following intravenous injection of anti-GLUT1 antibody-Fe_3O_4 NPs showed a significantly lower signal intensity than with unconjugated Fe_3O_4 NPs. This facilitated a more accurate differential diagnosis of infantile hemangioma from vascular malformation by MRI.

Concerning the hemangioma animal model used in the present study, it has already been demonstrated to be an identical model for animal studies of human infantile hemangioma.[12] Consistent with these previous reports, our model was identical to human infantile hemangioma in several ways, such as its histological features and the co-expression of GLUT1 and CD31.

A limitation of our study is the inability to investigate other sites in which GLUT1 is also expressed, such as brain endothelium, even if it cannot penetrate the blood brain barrier. We will investigate the localization of anti-GLUT1 antibody-Fe_3O_4 NPs at the brain endothelium in a further study. Another weakness of this study is that we did not perform a T2* map. However, we found a clear difference in signal intensity between the Fe_3O_4 NPs and the GLUT1 antibody-Fe_3O_4 NPs without the T2* map. The other weakness is that we did not evaluate anti-GLUT1 antibody-Fe_3O_4 NPs in the vascular malformation model. This is because the vascular malformation model is very difficult to construct and includes several types such as venous, capillary, lymphatic, and arteriovenous malformations.

This is the first study to develop a molecular imaging technique for the differential diagnosis of infantile hemangioma from vascular malformation that is feasible in T2*-weighted GRE MR images. This technique would be helpful for the differential diagnosis between infantile hemangioma and vascular malformation, especially when the differential diagnosis is difficult clinically, physically, and radiologically.

References

1. Gammpper TJ, Morgan RF. Vascular anomalies: hemangiomas. *Plast Reconstr Surg* 2002;**110**:572-85.
2. Bittles MA, Sidhu MK, Sze RW, Finn LS, Ghioni V, Perkins JA. Multidetector CT angiography of pediatric vascular malformationsand hemangiomas: utility of 3-D reformatting in differential diagnosis. *Pediatr Radiol* 2005;**35**:1100-6.
3. Bourrinet P, Bengele HH, Bonnemain B, Dencausse A, Idee JM, Jacobs PM, et al. Preclinical safety and pharmacokinetic profile of ferumoxtran-10, an ultrasmallsuperparamagnetic iron oxide magnetic resonance contrast agent. *Invest Radiol* 2006;**41**:313-24.
4. Swaminathan S, High WA, Ranville J, Horn TD, Hiatt K, Thomas M, et al. Cardiac and vascular metal deposition with high mortality in nephrogenic systemic fibrosis. *Kidney Int* 2008;**73**:1413-8.
5. Bulte JWM, Kraitchman DL. Iron oxide MR contrast agents for molecular and cellular imaging. *NMR Biomed* 2004;**17**:484-99.
6. Xie J, Liu G, Eden HS, Al H, Chen X. Surface-engineered magnetic nanoparticle platforms for cancer imaging and therapy. *Acc Chem Res* 2011;**44**:883-92.
7. Lee N, Hyeon T. Designed synthesis of uniformly sized iron oxide nanoparticles for efficient magnetic resonance imaging contrast agents. *Chem Soc Rev* 2012;**41**:2575-89.
8. Enjolras O, Wassef M, Chapot R. *Color atlas of vascular tumors and vascular malformations*. New York: NY Cambridge University Press; 2007.
9. Park J, An K, Hwang Y, Park JG, Noh HJ, Kim JY, et al. Ultra-large-scale syntheses of monodisperse nanocrystals. *Nat Mater* 2004;**3**:891-5.
10. Park YI, Kim JH, Lee KT, Jeon K, Na HB, Yu JH, et al. Nonblinking and nonbleaching upconverting nanoparticles as an optical imaging nanoprobe and T1 magnetic resonance imaging contrast agent. *Adv Mater* 2009;**21**:4467-71.
11. Paik JY, Lee KH, Ko BH, Choe YS, Choi Y, Kim BT. Nitric oxide stimulates 18 F-FDG uptake in human endothelial cells through increased hexokinase activity and GLUT1 expression. *J Nucl Med* 2005;**46**:365-70.
12. Tang Y, Liu W, Yu S, Wang Y, Peng Q, Xiong Z, et al. A novel in vivo model of human hemangioma: xenograft of human hemangioma tissue on nude mice. *Plast Reconstr Surg* 2007;**120**:869-88.

13. Hirshman MF, Goodyear LJ, Horton ED, Wardzala LJ, Horton ES. Exercise training increases GLUT-4 protein in rat adipose cells. *Am J Physiol* 1993;**264**:E882-9.

14. Coderre L, Vallega GA, Pilch PF, Chipkin SR. In vivo effects of dexamethasone and sucrose on glucose transport (GLUT-4) protein tissue distribution. *Am J Physiol* 1996;**271**:E643-8.

15. Chenevert TL, Sundgren PC, Ross BD. Diffusion imaging: insight to cell status and cytoarchitecture. *Neuroimaging Clin N Am* 2006;**16**:619-32 [viii-ix].

16. Cihangiroglu M, Ulug AM, Firat Z, Bayram A, Kovanlikaya A, Kovanlikaya I. High b-value diffusion-weighted MR imaging of normal brain at 3 T. *Eur J Radiol* 2009;**69**:454-8.

17. Gonzalez RG, Schaefer PW, Buonanno FS, Schwamm LH, Budzik RF, Rordorf G, et al. Diffusion-weighted MR imaging: diagnostic accuracy in patients imaged within 6 hours of stroke symptom onset. *Radiology* 1999;**210**:155-62.

18. Kim HJ, Choi CG, Lee DH, Lee JH, Kim SJ, Suh DC. High-b-value diffusion-weighted MR imaging of hyperacute ischemic stroke at 1.5 T. *AJNR Am J Neuroradiol* 2005;**26**:208-15.

Graphical Abstract

Nanomedicine: Nanotechnology, Biology, and Medicine xxx (2014) xxx

MRI molecular imaging using GLUT1 antibody-Fe$_3$O$_4$ nanoparticles in the hemangioma animal model for differentiating infantile hemangioma from vascular malformation

Chul-Ho Sohn, MD, PhD [a], Seung Pyo Park, PhD [b], Seung Hong Choi, MD, PhD [b], Sung-Hye Park, MD [c], Sukwha Kim, MD, PhD [d], Lianji Xu, MD, PhD [e], Sang-Hyon Kim, MD [f], Ji An Hur, MD, PhD [g], Jaehoon Choi, MD [h], Tae Hyun Choi, MD, PhD [d,*]

[a]Department of Radiology, Seoul National University College of Medicine, Seoul, Republic of Korea
[b]Center for Nanoparticle Research, Institute for Basic Science, and School of Chemical and Biological Engineering, Seoul National University, Seoul, Republic of Korea
[c]Department of Pathology, Seoul National University College of Medicine, Seoul, Republic of Korea
[d]Department of Plastic and Reconstructive Surgery, Institute of Human-Environment Interface Biology, Seoul National University College of Medicine, Seoul, Republic of Korea
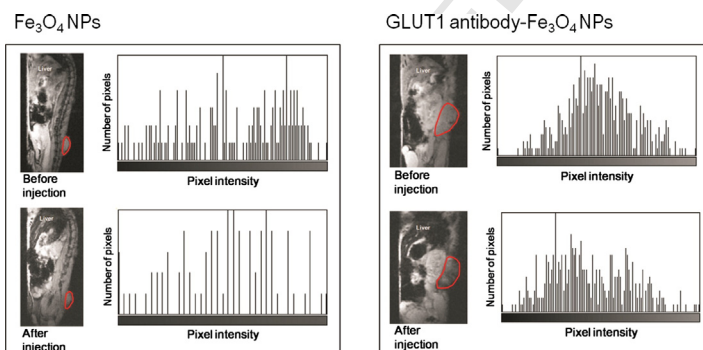[e]Department of Plastic and Reconstructive Surgery, Beijing Tongren Hospital, Capital Medical University, People's Republic of China
[f]Department of Internal Medicine, Keimyung University Dongsan Medical Center, Daegu, Republic of Korea
[g]Department of Internal Medicine, School of Medicine, Yeungnam University, Daegu, Republic of Korea
[h]Department of Plastic and Reconstructive Surgery, Keimyung University School of Medicine, Daegu, Republic of Korea

We developed glucose transporter protein 1 (GLUT1) antibody-conjugated iron oxide nanoparticles (Fe$_3$O$_4$ NPs) for the differential diagnosis of infantile hemangioma from vascular malformation that is feasible in T2*-weighted gradient-recalled-echo magnetic resonance (MR) images. In an in vivo mouse model of human infantile hemangioma, MRI imaging following intravenous injection of anti-GLUT1 antibody-Fe$_3$O$_4$ NPs showed a significantly lower signal intensity than with unconjugated Fe$_3$O$_4$ NPs. In hemangioma tissue excised 24 hours following the intravenous injection of anti-GLUT1 antibody-Fe$_3$O$_4$ NPs, Prussian blue-stained NPs were identified in CD31-positive endothelial cells of hemangioma: Figure 5.

AUTHOR QUERY FORM

ELSEVIER	**Journal: NANO** **Article Number: 985**	**Please e-mail or fax your responses and any corrections to:** **Elsevier** **E-mail: corrections.esi@elsevier.spitech.com** **Fax: 314-255-1425**

Dear Author,

Please check your proof carefully and mark all corrections at the appropriate place in the proof (e.g., by using on-screen annotation in the PDF file) or compile them in a separate list. Note: if you opt to annotate the file with software other than Adobe Reader then please also highlight the appropriate place in the PDF file. To ensure fast publication of your paper please return your corrections within 48 hours.

For correction or revision of any artwork, please consult http://www.elsevier.com/artworkinstructions.

Any queries or remarks that have arisen during the processing of your manuscript are listed below and highlighted by flags in the proof. Click on the 'Q' link to go to the location in the proof.

Location in article	Query / Remark: **click on the Q link to go** **Please insert your reply or correction at the corresponding line in the proof**
Q1	Please confirm that given names and surnames have been identified correctly.
Q2	Abstract exceeds the maximum word limit [150]. Please modify accordingly. Please check this box if you have no corrections to make to the PDF file. ☐

Thank you for your assistance.